Model energy landscapes of low-temperature fluids: Dipolar hard spheres

Dmitry V. Matyushov*
Center for Biological Physics, Arizona State University, P.O. Box 871604, Tempe, Arizona 85287-1604, USA
(Received 2 January 2007; revised manuscript received 5 March 2007; published 24 July 2007)

An analytical model of non-Gaussian energy landscape of low-temperature fluids is developed based on the thermodynamics of the fluid of dipolar hard spheres. The entire excitation profile of the liquid, from the high-temperature liquid to the point of ideal-glass transition, has been obtained from Monte Carlo simulations. The fluid of dipolar hard spheres loses stability close to the point of ideal-glass transition transforming via a first-order transition into a columnar liquid phase of dipolar chains locally arranged in a body-centered-tetragonal order. Significant non-Gaussianity of the energy landscape is responsible for narrowing of the distribution of potential energies and energies of inherent structures with decreasing temperature. We suggest that the proposed functionality of the enumeration function is widely applicable to both polar and nonpolar low-temperature liquids.

DOI: 10.1103/PhysRevE.76.011511 PACS number(s): 64.70.Pf, 65.40.Gr, 66.20.+d

I. INTRODUCTION

Thermodynamic and dynamic properties of supercooled liquids are often related to the excess of configurations they possess relative to the crystalline phase [1]. The number of states of the liquid state is reflected by the configurational entropy $S_c(T)$ (in k_B units) conventionally defined [2–5] as the logarithm of the density of states $\Omega(E)$ taken at the potential energy $E(T)$ of an N-particle system at temperature T,

$$S_c(T) = \ln\{\Omega[E(T)]\}. \tag{1}$$

The energy integral of the density of states with the Boltzmann factor gives the canonical configuration integral

$$Z(\beta) = \int \Omega(E) e^{-\beta E} dE, \tag{2}$$

where β is the inverse temperature.

Stillinger [6,7] gave an alternative definition of the configurational entropy in terms of the density of states $\Omega_\phi(\phi)$ of inherent structures, i.e., minima of the total energy of the system as a function of all its translational and rotational degrees of freedom (energy landscape). Here, $\phi=\Phi/N$ is the minimum depth on a per-particle basis [6] and N is the number of liquid particles. The canonical configuration integral is now given by integrating over the basin depths ϕ and the free energy of interbasin vibrations $F_v(\phi)$, which is a weak, approximately linear, function of ϕ [8,9]

$$Z(\beta) = \int d\phi \Omega_\phi(\phi) e^{-\beta N\phi - \beta F_v(\phi)}. \tag{3}$$

Because of the central role of the configurational entropy in early theories of viscous liquids by Adam, Gibbs, and DiMarzio [2,10], and more recent random first-order transition models by Wolynes and co-workers [11,12], much effort has been invested in calculating the Stillinger configurational entropy, $S_c^\phi(T)=\ln\{\Omega_\phi[\phi(T)]\}$, from computer simulations of model fluids [8,9,13]. A general connection between $S_c(T)$ and $S_c^\phi(T)$ is, however, still unclear.

Analytical modeling of the landscape of supercooled liquids is to a large extent based on the ideas advanced for spin glasses with quenched disorder [14,15]. The most prominent role in application to structural glasses is played by Derrida's random energy, or Gaussian landscape, model (REM) [16]. Computer simulations, mostly limited to temperatures above the mode-coupling critical temperature, basically support the REM, in particular the prediction of the $1/T$ falloff of the average basin energy $\phi(T)$ from its high-temperature plateau [8,9]. However, general theoretical arguments [7,17] and recent simulations [13] suggest that the low-energy portion of the Gaussian landscape might be inaccurate. In particular, combinatorial arguments suggest that the derivative of the enumeration function, $\sigma_\phi(\phi)=N^{-1}\ln[\Omega_\phi(\phi)]$, approaches infinity at the point of ideal-glass transition when the system runs out of configurations and $\sigma_\phi(\phi_{\rm IG})=0$. This infinite derivative eliminates the ideal-glass transition at a positive temperature [7]. A phenomenological description, patching together logarithmic and Gaussian enumeration functions, was suggested to provide a correct low-energy portion of $\sigma_\phi(\phi)$ [18].

Generally, unlike the case of spin glasses, there has been a lack of simple, solvable models of structural glass formers. In this paper we propose a model of non-Gaussian landscape of low-temperature fluids with no quenched disorder. Our derivation is based on the established thermodynamics of the model fluid of dipolar hard spheres (DHS) [19]. This monatomic glass former (in contrast to binary mixtures used in many recent simulations [8,9]) is long known to resist liquid-gas and liquid-crystal phase transformations, although it shows orientational order-disorder transitions. This fluid lacks the liquid-vapor transition decomposing instead into low-density dipolar chains [20,21]. Upon cooling, it transforms into a ferroelectric fluid [22], but the ferroelectric phase is stabilized by tin-coil boundary conditions used in simulations [23] and can be prevented by using a low dielectric constant for the reaction-field or Ewald corrections for the cutoff of dipolar interactions [24]. This strategy has been

*dmitrym@asu.edu

employed in this study, which has allowed us to obtain the energy profile of the fluid phase down to the point of order-disorder phase transition which appears to be close to the temperature of the ideal-glass transition.

II. MONTE CARLO SIMULATIONS

We have carried out Monte Carlo (MC) simulations of the DHS fluid within the standard *NVT* Metropolis protocol with the minimum image convention and the cutoff of dipolar interactions at one-half of the box length. The initial configuration was set up as a face-centered-cubic (fcc) lattice of $N=108$ dipolar spheres used at the beginning of all simulations at different temperatures. The cubic simulation box helps to suppress crystallization of dipoles which do not favor highly symmetric lattice structures [25,26]. The long-range part of dipolar interactions was taken into account with the reaction-field corrections. The reaction-field dielectric constant of $\epsilon_{RF}=10$, below the lowest value $\simeq 18$ permitting the ferroelectric phase [24], has allowed us to eliminate the transition to liquid ferroelectric. The data were collected for $(2-10)\times 10^7$ MC cycles. The small size of the simulation box is required for the sampling of the low-temperature fluid phase found in this paper and also to be able to determine the statistics of the energy fluctuations the variance of which scales as $1/\sqrt{N}$ with the number of particles [8]. The relatively small size of the simulation box does not, however, significantly affect the energy values. For instance, the energies of DHS fluids at reduced dipole moments $(m^*)^2=\beta m^2/\sigma^3$ equal to $(m^*)^2=1.0$ and 2.0 are $\beta E/N=-1.01$ and -2.725 for $N=108$ particles and $\beta E/N=-1.01$ and -2.753 [27] for $N=256$ at $\rho^*=\rho\sigma^3=0.8$. Here, ρ is the number density, σ is the hard-sphere diameter, and m is the dipole moment.

III. ENUMERATION FUNCTION

Apart from avoiding crystallization, a significant advantage of the DHS fluid is the existence of a simple analytical form for the excess (over the ideal gas) free energy $\beta F(\beta)=-\ln[Z(\beta)]$. The Padé truncation of perturbation series suggested by Stell and co-workers [28] turned out to be very successful when tested against simulations [19]. The free energy of dipolar hard spheres depends on two parameters, the reduced density $\rho^*=\rho\sigma^3$ and the reduced temperature $T=k_BT\sigma^3/m^2$. All calculations and simulations here have been done at constant volume with $\rho^*=0.8$ thus reducing the number of variables to one.

Stell's Padé solution for $F(\beta)$ is

$$\beta F(\beta)=Nf(\eta)-\frac{A\beta^2}{1+b\beta}. \tag{4}$$

Here $f(\eta)$ is the reduced free energy of the fluid of hard spheres with zero dipole moment as a function of the packing density $\eta=(\pi/6)\rho^*$. For the Carnahan-Starling equation of state, one has $f(\eta)=(4\eta-3\eta^2)/(1-\eta)^2$. $\beta=1/T$ in Eq. (4) is given in reduced units and thus the coefficients $A=Na$ and b depend only on the liquid density through two-particle and three-particle perturbation integrals, $a=(\rho^*/6)I^{(2)}(\rho^*)$, $b=(\rho^*/9)I^{(3)}(\rho^*)/I^{(2)}(\rho^*)$, tabulated by Larsen *et al.* [28]. These coefficients, taken at $\rho^*=0.8$, were used in the calculations of the configurational thermodynamics.

Stell's Padé form for the free energy interpolates between two well-established limits, the high-temperature expansion in the dipole-dipole interaction, which starts from $-A\beta^2$ term, and the low-temperature saturation limit [29,30], $\beta F(\beta)\propto-\beta$. The high-temperature limit gives Gaussian statistics of the energy fluctuations and the Gaussian top of the energy landscape, while the low-temperature asymptote will produce the non-Gaussian portion of the energy landscape.

Following Freed [5], the density of states can be obtained by inverse Laplace transformation of Eq. (2) in which we use $\beta F(\beta)$ in the Padé form given by Eq. (4). This transformation will produce the enumeration function depending on the potential energy, in contrast to the energy of inherent structures used in Stillinger's formulation. The inverse Laplace transform is calculated by expanding $\exp[-\beta F(\beta)]$ in powers of the second summand in Eq. (4) and performing pole integration. The result can be converted to a closed-form equation,

$$\Omega(e)=(b\sqrt{1+e/c})^{-1}\exp[-Nf(\eta)-N(e+2c)/b]\times I_1[(2cN/b)\sqrt{1+e/c}], \tag{5}$$

where $c=a/b$, $I_1(x)$ is the first-order modified Bessel function, and $e=E\sigma^3/Nm^2$ is the reduced internal energy per particle. Since the argument of the Bessel function in Eq. (5) is proportional to the number of particles N, its thermodynamic-limit expansion gives the following expression for the enumeration function $\sigma(e)=N^{-1}\ln[\Omega(e)]$:

$$\sigma(e)=s_0-b^{-1}(\sqrt{c+e}-\sqrt{c})^2, \tag{6}$$

where s_0, which requires separate definition, gives the top of the energy landscape corresponding to the hard-sphere liquid with zero potential energy.

The enumeration function in Eq. (6) is Gaussian near its top, $e\simeq 0$, where the dipole-dipole interactions are insignificant and can be considered as a small perturbation to the limit of a hard-sphere fluid:

$$\sigma^G(e)=s_0-e^2/(4cb). \tag{7}$$

The enumeration function deviates from the parabolic shape in its low-energy wing, in particular close to the low-energy cutoff at $e_0=-c$ [Fig. 1(a)]. The average energy, configurational entropy, and configurational constant-volume heat capacity $c_V(T)$ (in k_B units) can be obtained from the following thermodynamic identities [31]:

$$[\partial\sigma(e)/\partial e]|_{e(T)}=\beta,$$

$$[\partial\sigma^2(e)/\partial e^2]|_{e(T)}=-\beta^2/c_V, \tag{8}$$

where the first and second derivatives are taken at the average potential energy per particle $e(T)=\sigma^3E(T)/(m^2N)$.

The application of Eq. (8) to Eq. (6) leads to the following equations for the average energy:

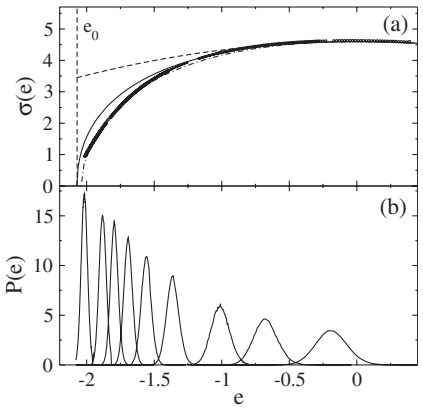

FIG. 1. Enumeration function $\sigma(e)$ (a) and distribution functions $P(e)$ (b) of the fluid of dipolar hard spheres at $\rho^*=0.8$ and the temperatures T [from left to right in (b)]: 0.125, 0.167, 0.2, 0.25, 0.33, 0.5, 1.0, 2.0, 10.0. The simulation points in (a) are obtained from functions $P(e)$ within 95% of the maximum probability at each temperature according to Eq. (12). The dashed line in (a) indicates the Gaussian enumeration function given by Eq. (7) and the solid line is calculated from Eq. (6) with $s_0=4.6$ and $a=0.9345$ and $b=0.4509$ from the perturbation expansion [28,30]. The dashed-dotted line, almost indistinguishable from the simulation points in (a), is the result of the fit of Eq. (6) to the simulated enumeration function using a and b as fitting parameters. The best-fit values are $a=0.7839$ and $b=0.3790$. The vertical dashed line in (a) indicates the cutoff energy $e_0=-2.07$.

$$e(T) = -c + c(1+\beta b)^{-2}, \tag{9}$$

configurational entropy per particle $s_c(T)=S_c(T)/N$,

$$s_c(T) = s_0 - [c_V^G(T)/2](1+\beta b)^{-2}, \tag{10}$$

and configurational (constant-volume) heat capacity per particle,

$$c_V(T) = c_V^G(T)(1+\beta b)^{-3}. \tag{11}$$

In Eqs. (10) and (11), $c_V^G(T)=2\beta^2 cb$ is the heat capacity of the Gaussian landscape.

Depending on the parameters, Eq. (10) gives two possible resolutions of the entropy crisis of low-temperature fluids [1]. When $s_c(0)=s_0-c/b\geqslant 0$, the enumeration function has an infinite derivative at e_0 and, according to Stillinger's arguments [7], there is no ideal-glass transition. When $s_c(0)$ is strictly positive, the entropy is nonzero at the cutoff energy, a situation observed for network glass formers [32]. Finally, when $s_c(0)<0$, the ideal-glass arrest $\sigma(e_{\mathrm{IG}})=0$ happens before the cutoff is reached, and the temperature of ideal-glass transition T_{IG} $[e_{\mathrm{IG}}=e(T_{\mathrm{IG}})]$ is positive.

The configurational entropy of the hard-sphere fluid, which strongly affects which one of these scenarios will materialize, has been discussed in the literature [33–35]. Speedy's [33] estimate of the configurational entropy at $\rho^*=0.8$ gives $s_0\simeq 1.7$, in good agreement with more recent calculations by Angelani *et al.* [35]. However, when this entropy magnitude is used in Eq. (6), the energy minimum e_{IG} is above the energy cutoff $e_0=-c$ which we could actually reach in our simulations. Since this energy is the lowest energy we could observe for the isotropic phase (see below), we use the energy cutoff e_0 as the lowest energy, $e_0=e_{\mathrm{IG}}$, which makes $s_0=c/b\simeq 4.6$. This choice also eliminates the ideal-glass transition at a positive temperature from the analytical model and results in $T_{\mathrm{IG}}=0$. Note that configurational entropies above Speedy's estimate were also reported in Ref. [13] for a fluid of hard spheres with square-well attraction.

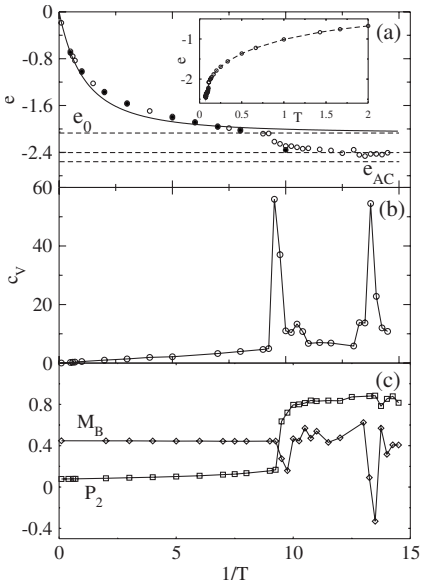

FIG. 2. Average potential energy $e(T)$ (a), constant-volume heat capacity c_V (b), and the nematic (P_2, squares) and Binder (M_B, diamonds) parameters (c) vs $1/T$. The points in (a) are the results of MC simulations: open points for the potential energies and close points for the energies of inherent structures. The solid line in (a) shows the Padé approximation of Eq. (9) with the parameters c and b calculated from the perturbation expansion. The dashed horizontal lines show the cutoff energy $e_0=-2.07$, the energy of noninteracting dipolar chains $e=-2.4$ (middle line), and the energy of the closed-packed fcc antiferroelectric crystal $e_{AC}=-2.56$. The inset in (a) shows $e(T)$ from MC simulations.

The enumeration function from Eq. (6) is compared to the results of MC simulations in Fig. 1(a). The simulation points were obtained by patching together central parts (within 95% of the maximum magnitude) of normalized distribution functions $P(e)$ at different temperatures according to the equation

$$\sigma(e) = N^{-1}\ln[P(e)] + \beta e - \beta F(\beta)/N, \tag{12}$$

where $F(\beta)/N$ is obtained from the numerical integration of the simulated $e(\beta)$ dependence [Fig. 2(a)]. All curves are shifted by the same temperature-independent constant to match s_0 at the top of the landscape.

The density of states from simulations deviates downward from Eq. (6) in its lower portion, on approach to the ideal-glass state. This trend results in a slightly shallower temperature drop of $e(T)$ from simulations compared to the result of the Padé approximation in Eq. (9) [cf. points to the solid line in Fig. 2(a)]. Also shown in Fig. 1(a) is the Gaussian enumerations function from Eq. (7) (dashed line). Even though a better fit of the simulation data can of course be obtained by varying the Gaussian curvature, Fig. 1(a) shows that the ex-

trapolation of the high-temperature Gaussian statistics to low temperatures results in very inaccurate predictions for the landscape thermodynamics.

The non-Gaussian form of $\sigma(e)$ forces the width of $P(e)$ to decrease with cooling [Fig. 1(b)]. This behavior is quite distinct from the prediction of the Gaussian landscape model in which the width is temperature independent [16]. The temperature dependence of the width is directly related to the heat capacity since

$$P(e) \propto \exp\left(-N\frac{(\delta e)^2}{2c_V^{\mathrm{ex}}(T)T^2}\right), \tag{13}$$

where $\delta e=\sigma^3[E-E(T)]/(m^2N)$ is the energy fluctuation and $c_V^{\mathrm{ex}}(T)$ is the excess constant-volume heat capacity over that of the ideal gas,

$$c_V^{\mathrm{ex}}(T)=\frac{\langle(\delta E)^2\rangle}{N(k_BT)^2}. \tag{14}$$

According to Eqs. (8) and (12), $c_V^{\mathrm{ex}}(T)$ is equal to the configurational heat capacity $c_V(T)$.

The high-temperature portion of the heat capacity, corresponding to the distributions shown in Fig. 1(b), scales linearly with the inverse temperature, $c_V(T)\propto 1/T$ [Fig. 2(b)]. This hyperbolic temperature scaling, often documented for structural glass formers at constant pressure [36], results in a linear temperature scaling of the squared width when the distribution $P(e)$ is fitted to a Gaussian function. This behavior was previously predicted by models of supercooled liquids in terms of configurational excitations [17,37].

The calculation of the energies of inherent structures by conjugate gradient minimization of configurations along simulated trajectories results in reduced energies $\phi(T)$ just slightly below $e(T)$ [closed points in Fig. 2(a)]. This means that the long-range dipolar forces produce essentially a mean-field potential for the local translations and rotations, and Eq. (6) for the density of internal energies can be used for the density of inherent structures as well, $\Omega(e)\simeq\Omega_\phi(e)$.

The configurational entropy was obtained from the simulated heat capacity according to the thermodynamic integration

$$s_c(T)=s_0-\int_T^\infty [c_V(T')/T']dT'. \tag{15}$$

This function is compared to $s_c(T)$ from Eq. (10) in Fig. 3(a). According to the choice of s_0 the analytical configurational entropy crosses zero at $T_{\mathrm{IG}}=0$. On the contrary, the simulated configurational entropy is steeper in its low-temperature portion resulting in a positive T_{IG}. The heat capacity obtained from MC simulations according to Eq. (14) compares well to the analytical expression in Eq. (11) at relatively high temperatures, but starts to deviate significantly upward with lowering temperature [Fig. 3(b)]. In contrast, analytical $c_V(T)$ passes through a maximum at $T_{\max}=b/2$ and decays to zero as $\propto T$ at lower temperatures.

The upward deviation of the heat capacity from the analytical result is caused by what is not a part of the analytical theory—the loss of stability of the DHS fluid and the occurrence of a first-order transition at the temperature T_{IG} when $s_c(T)$ crosses the zero line and an ideal-glass transition is expected [cf. Fig. 3(a) and 3(b)]. The DHS fluids thus lose stability when it runs out of configurations and transforms via a first-order liquid-liquid transition into a low-temperature phase.

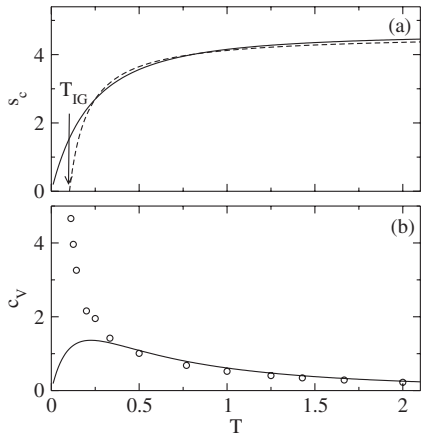

FIG. 3. Configurational entropy (a) and constant-volume heat capacity (b) vs reduced temperature. The solid line in (a) is the result of the analytical model with the parameters b and c in Eq. (10) calculated from the perturbation expansion. The dashed line is obtained according to Eq. (15) from the constant-volume heat capacity obtained from MC simulations. The vertical arrow indicates the ideal-glass temperature T_{IG}. In (b), the solid line is calculated from Eq. (11) and the points are from MC simulations at $\rho^*=0.8$ [Eq. (14)].

IV. LOW-TEMPERATURE PHASE

Instead of leveling off while approaching the cutoff energy $e_0=-2.07$, the average energy drops discontinuously to approximately the energy of a particle within an infinite dipolar chain with all dipoles aligned along the chain axis [38]: $e=-2.40$ [middle dashed line in Fig. 2(a)]. Since the interaction energy of two infinite dipolar chains is an oscillatory function of their parallel displacement [38], this energy also corresponds to an ensemble of randomly displaced chains of dipoles and is slightly above the energy of a close-packed antiferroelectric fcc crystal $e_{AC}=-2.56$ [39]. The drop of the average energy at T_{IG} marks the first-order liquid-liquid transition accompanied by a sharp peak in the heat capacity [Figs. 2(a) and 2(b)]. The orientational structure of the fluid also changes as indicated by a stepwise increase in the nematic order parameter P_2 [Fig. 2(c)] calculated as the largest eigenvalue of the $\mathbf{Q}$ tensor,

$$\mathbf{Q}=(2N)^{-1}\sum_j(3\hat{\mathbf{e}}_j\hat{\mathbf{e}}_j-\mathbf{I}), \tag{16}$$

where $\hat{\mathbf{e}}_j$ is a unit vector along the dipole of particle j. The ferroelectric order parameter P_1 (normalized total dipole moment of the liquid $\mathbf{M}$) remains close to zero, i.e., the liquid remains unpolarized. The Binder parameter [40], $M_B=1-\langle\mathbf{M}^4\rangle/3\langle\mathbf{M}^2\rangle^2$, also shows downward spikes [Fig. 2(c)] pointing to the first-order character of the first transition and,

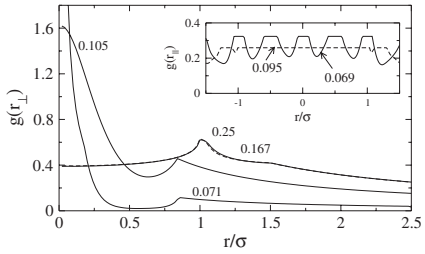

FIG. 4. Pair distribution function of transverse interparticle separations (relative to the nematic director) at temperatures indicated in the plot. The high-temperature results for $T=0.167$ (dashed line) and $T=0.25$ (solid line) almost coincide on the scale of the plot. The distribution of distances parallel to the director in the inset shows the transition to the smectic phase of parallel chains with the local bct order. The temperatures indicated in the inset are above ($T=0.095$) and below ($T=0.069$) the nematic-smectic transition.

even more sharply, of the second one which we discuss shortly.

The properties of the low-temperature fluid phase are peculiar. Both the density ($\propto\langle|\rho_k|^2\rangle$) and polarization ($\propto\langle|M_k|^2\rangle$) structure factors do not show crystalline spatial or orientational order. However, snapshots of simulated configurations (not shown here) indicate the existence of chains of dipoles aligned head-to-tail. These chains are persistent for $(5-20)\times10^3$ MC cycles resulting in the overall slow convergence of simulations in the low-temperature phase. The chains of parallel dipoles are arranged in bundles with the locally body-centered-tetragonal (bct) structure in which two adjacent chains are displaced relative to each other by the hard-sphere radius. This arrangement has the lowest energy for fluids forming columnar phases of parallel, ferroelectrically ordered chains of dipoles [38,41]. A body-centered orthorhombic lattice was suggested as the ground state for Stockmayer ferroelectrics [25]. In the present case, all the chain bundles are parallel to the same director, but the net moment is compensated among the oppositely oriented bundles.

The columnar structure is well seen in the pair correlation function of transverse separations, which is very sensitive to columnar order [42] (Fig. 4). At the phase transition, a peak at zero transverse projection indicates the emergence of the columnar phase. At the same time, a smaller peak, present at $r/\sigma=1$ in the isotropic dipolar fluid, shifts to $r/\sigma=\sqrt{3}/2$ characteristic of the closest bct distance [38]. The one-dimensional dipolar chains experience strong Landau-Peierls fluctuations with the orthogonal mean-square displacement scaling as $\langle r_\perp^2\rangle\propto lT$ [43], where l is the average length of the chain. The fits of the initial portion of the $g(r_\perp)$ result is almost invariant $\langle r_\perp^2\rangle\simeq0.07\sigma^2$ suggesting that the length of the chains increases as $1/T$.

The nematic columnar phase transforms into a smectic phase with further cooling as indicated by the second peak of the heat capacity [Fig. 2(b)], a downward spike of the Binder parameter [Fig. 2(c)], and the appearance of clear density modulation in the distribution function of molecular separations parallel to the director (inset in Fig. 4). A similar smectic phase has been previously observed for much smaller dipole magnitudes in fluids of disklike dipolar particles (cut spheres) [44].

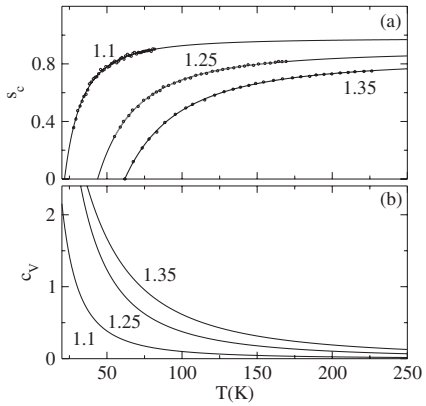

FIG. 5. Configurational entropy (a) and configurational heat capacity (b) of the BLJM fluid. The dots are simulation results of Sastry [9] and the solid lines are the results of the fit to Eq. (6) in which s_0, $c=a/b$, and b are considered as fitting parameters. The fit has been done at three reduced densities $\rho^*=\rho/\rho_0$ of the BLJM fluid indicated in the plot, $\rho_0=1.678$ g/cm^3. The argon energy scale is used to convert from dimensionless energies to units of kelvin. The fitting parameters $\{s_0,c,b\}$ are {0.977,407.5,1.272}, {0.890,320.4,7.228}, and {0.828,447.2,9.409} for $\rho^*=1.1$, 1.25, and 1.35, respectively; c and b parameters are given in units of kelvin.

V. LANDSCAPE MODEL

The calculations of the landscape thermodynamics of the DHS fluid in this paper have been done with the constants $A=aN$ and b in Eq. (4) taken from the perturbation expansion in respect to the reference fluid of hard spheres [28]. Equation (6) can alternatively be considered as a general non-Gaussian landscape model with three parameters varied to analyze the data of simulations or the laboratory experiment. In fact, an about 20% change in the parameters a and b allows a very close fit of Eq. (6) to the enumeration function from our simulations [dashed-dotted line in Fig. 1(a)]. It is interesting to ask whether this landscape model can fit the previously reported configurational thermodynamics of binary Lennard-Jones mixture (BLJM) models [8,9], in particular since the Gaussian REM model has often been used to rationalize the observations [9,45].

Figure 5(a) shows the fit of Eq. (10) to Sastry's [9] configurational entropies of the BLJM liquid. The corresponding constant-volume heat capacities are given in Fig. 5(b). Since the energy and temperature are now measured in units of kelvin, c and b parameters have the same units. The values of the fitting parameter $c\simeq320-450$ K turns out to be significantly larger than the energy scale available from simulations, $|e|\simeq10$ K ($b\simeq1-10$ K). The enumeration function of the BLJM fluid can then be obtained by a series expansion in e/c in Eq. (6) and is essentially Gaussian [Eq. (7)]. This observation is in agreement with available simulation data [8,46].

The agreement with simulations shown in Fig. 5 may be not coincidental. According to perturbation theories of non-

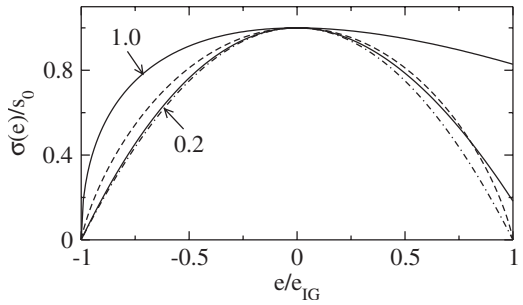

FIG. 6. Reduced enumeration function $\sigma(e)/s_0$ vs e/e_{IG} for the Gaussian (dashed-dotted line), logarithmic [dashed line, Eq. (17)], and present [solid lines, Eq. (18)] models. e_{IG} is the energy at which the enumeration function becomes zero, $\sigma(e_{\mathrm{IG}})=0$. The solid lines are calculated at the values of $|e_{\mathrm{IG}}|/c$ shown in the plot.

polar liquids [47], the high-temperature heat capacity is caused by the second-order expansion term in the free energy $\beta F(\beta) \propto \beta^2$, as is also suggested by Eq. (4). It is reasonable to expect that the energy of a LJ fluid at a given density will have a lower boundary with decreasing temperature. The free energy will then scale as $\beta F(\beta) \propto \beta$ as in the Padé form in Eq. (4). For substances with electrostatic interactions, the free energy of any liquid with anisotropic potential is expected to scale as $\beta F(\beta) \propto \beta^2$ at high temperatures (perturbation expansion [19]) and, following Onsager's arguments [29], should saturate to a linear scaling $\beta F(\beta) \propto \beta$ at low temperatures. Since capturing these two limits is the main thrust of the Padé formula, we expect that the proposed functionality for the enumeration function [Eq. (6)] is universal for both polar and nonpolar liquids within uncertainties possibly introduced by Padé interpolation.

It is instructive to compare the enumeration functionality proposed by the present model with other functional forms existing in the literature. Following Shell and Debenedetti [48], we consider the reduced function $f(\rho, e_{\mathrm{IG}}, e)=\sigma(e)/s_0$ depending on the liquid density and the minimum energy e_{IG} at which the enumeration function crosses the zero level, $\sigma(e_{\mathrm{IG}})=0$ ($s_0 \leqslant c/b$ in the present model). The dependence on ρ disappears in the Gaussian model in which this reduced function depends only on the ratio $u=e/e_{\mathrm{IG}}$, $f^G(u)=1-u^2$. Similar independence of density is assumed in the logarithmic model [48],

$$f[u] = 1 - (\ln[4])^{-1}[(1-u)\ln(1-u) + (1+u)\ln(1+u)]. \tag{17}$$

In contrast, in the present model, the dependence on density is generally preserved through the parameter $c=c(\rho^*)$,

$$f(\rho, e_{\mathrm{IG}}, e) = 1 - \left(\frac{\sqrt{1+e/c}-1}{\sqrt{1+e_{IG}/c}-1} \right)^2. \tag{18}$$

When $|e_{\mathrm{IG}}| \ll c$, as is the case for the BLJM fluid ($|e_{\mathrm{IG}}|/c \simeq 0.25$), Eq. (18) reduces to the Gaussian landscape. The comparison of Gaussian and logarithmic functions to Eq. (18) is given in Fig. 6.

Significant non-Gaussianity of the energy landscape of the DHS fluid causes a noticeable, approximately linear, temperature dependence of the squared Gaussian width of the distribution of energies and inherent structures. The energy distribution is non-Gaussian and a temperature-dependent width needs to be introduced when it is represented by a Gaussian function. The linear temperature scaling of the squared distribution width was previously predicted by the model of thermodynamics of low-temperature glass formers in terms of configurational excitations with the Gaussian statistics of excitation energies [17,37]. That model also predicted fragile glass formers to release the excess of their configurational entropy through first-order transitions usually hidden below the glass transition. Both an approximately linear temperature dependence of the width and the occurrence of the first-order transition are confirmed by our present simulations of the DHS fluid. The analytical model developed here lacks, however, the phase transition. This result is expected since the Padé form of the free energy describes the high-temperature phase only. The discontinuous liquid-liquid transition can be introduced via cooperative two-state models [49] since properties of both phases are known from simulations.

VI. CONCLUSIONS

In conclusion, we have developed a non-Gaussian landscape model of low-temperature fluids which is based on Padé interpolation between high-temperature quadratic and low-temperature linear scalings of the liquid free energy with β. The model has been tested on simulations of the DHS fluid and shows a good agreement with simulated configurational thermodynamics almost down to the temperature of ideal-glass transition. The DHS liquid nearly avoids the ideal-glass state through a liquid-liquid transition thus resolving the Kauzmann paradox [1] through phase transformation. This last statement is, however, bound to the assumption that the configurational entropy vanishes at the cutoff energy e_0, which has already placed the top of the enumeration function above the known estimates for the configurational entropy of hard-sphere fluids [33,35]. If this entropy is even higher, an alternative scenario appears: the liquid never reaches the ideal-glass state and the orientational order-disorder transition happens at the point where the configurational entropy is about to inflect into a constant value extending down to $T=0$ (as observed in Ref. [13]).

Our simulations have added yet another example to the list of previously observed liquid-liquid transitions in glass-forming substances [1,50–53]. The present system is particularly interesting since we could equilibrate it down to almost the ideal-glass temperature apparently without reaching the kinetic arrest. This feature might allow one to test the connection between dynamic slow down and configurational entropy advocated by the Adam-Gibbs theory [2] once relaxation data have become available for the DHS fluid.

The appearance of thermodynamically stable chainlike column inhomogeneities in the low-temperature phase may shed more light on the discussion of analogous, thermodynamically unstable, excitations in supercooled liquids above

the glass transition [54–57]. In particular, it has been suggested that forces and displacements are transmitted in low-temperature liquids primarily along one-dimensional structures [56,58,59]. Our present simulations extend this notion to anisotropic liquids suggesting that orientational excitations are also transmitted along one-dimensional chains. These excitations, which should exist as thermal excitations in the high-temperature phase, constitute a soft (Goldstone) mode which condenses into thermodynamically stable structures in the low-temperature phase.

ACKNOWLEDGMENTS

This research was supported by the NSF (Grant No. CHE-0616646). The author is grateful to Vitaliy Kapko for helpful comments on this paper.

[1] C. A. Angell, K. L. Ngai, G. B. McKenna, and S. W. Martin, J. Appl. Phys. **88**, 3113 (2000).
[2] G. Adam and J. H. Gibbs, J. Chem. Phys. **43**, 139 (1965).
[3] I. M. Lifshitz, A. Y. Grosberg, and A. R. Khokhlov, Rev. Mod. Phys. **50**, 683 (1978).
[4] J. D. Bryngelson and P. G. Wolynes, Proc. Natl. Acad. Sci. U.S.A. **84**, 7524 (1987).
[5] K. F. Freed, J. Chem. Phys. **119**, 5730 (2003).
[6] F. H. Stillinger and T. A. Weber, Phys. Rev. A **25**, 978 (1982).
[7] F. H. Stillinger, J. Chem. Phys. **88**, 7818 (1988).
[8] S. Büchner and A. Heuer, Phys. Rev. E **60**, 6507 (1999).
[9] S. Sastry, Nature (London) **409**, 164 (2001).
[10] J. H. Gibbs and E. A. D. Marzio, J. Chem. Phys. **28**, 373 (1958).
[11] X. Xia and P. G. Wolynes, Proc. Natl. Acad. Sci. U.S.A. **97**, 2990 (2000).
[12] J. D. Stevenson, J. Schmalian, and P. G. Wolynes, Nat. Phys. **2**, 268 (2006).
[13] A. J. Moreno, I. Saika-Voivod, E. Zaccarelli, E. L. Nave, S. V. Buldyrev, P. Tartaglia, and F. Sciortino, J. Chem. Phys. **124**, 204509 (2006).
[14] M. Mezard, G. Parisi, and M. Virasoro, *Spin Glass Theory and Beyond* (World Scientific, Singapore, 1987).
[15] T. R. Kirkpatrick, D. Thirumalai, and P. G. Wolynes, Phys. Rev. A **40**, 1045 (1989).
[16] B. Derrida, Phys. Rev. B **24**, 2613 (1981).
[17] D. V. Matyushov and C. A. Angell, J. Chem. Phys. **123**, 034506 (2005).
[18] P. G. Debenedetti, F. H. Stillinger, and M. S. Shell, J. Phys. Chem. B **107**, 14434 (2003).
[19] C. G. Gray and K. E. Gubbins, *Theory of Molecular Liquids* (Clarendon, Oxford, 1984).
[20] J. J. Weis and D. Levesque, Phys. Rev. Lett. **71**, 2729 (1993).
[21] M. E. van Leeuwen and B. Smit, Phys. Rev. Lett. **71**, 3991 (1993).
[22] D. Wei and G. N. Patey, Phys. Rev. Lett. **68**, 2043 (1992).
[23] I. Ponomareva, I. I. Naumov, I. Kornev, H. Fu, and L. Bellaiche, Phys. Rev. B **72**, 140102(R) (2005).
[24] D. Wei, G. N. Patey, and A. Perera, Phys. Rev. E **47**, 506 (1993).
[25] G. T. Gao and X. C. Zeng, Phys. Rev. E **61**, R2188 (2000).
[26] B. Groh and S. Dietrich, Phys. Rev. E **63**, 021203 (2001).
[27] D. V. Matyushov and B. M. Ladanyi, J. Chem. Phys. **110**, 994 (1999).
[28] B. Larsen, J. C. Rasaiah, and G. Stell, Mol. Phys. **33**, 987 (1977).
[29] L. Onsager, J. Phys. Chem. **43**, 189 (1939).
[30] G. Stell, in *Statistical Mechanics. Part A: Equilibrium Techniques*, edited by B. J. Berne (Plenum, New York, 1977).
[31] L. D. Landau and E. M. Lifshits, *Statistical Physics* (Pergamon, New York, 1980).
[32] A. Saksaengwijit, J. Reinisch, and A. Heuer, Phys. Rev. Lett. **93**, 235701 (2004).
[33] R. J. Speedy, Mol. Phys. **95**, 169 (1998).
[34] G. Parisi and F. Zamponi, J. Chem. Phys. **123**, 144501 (2005).
[35] L. Angelani, G. Foffi, and F. Sciortino, e-print arXiv:cond-mat/0506447.
[36] R. Richert and A. C. Angell, J. Chem. Phys. **108**, 9016 (1998).
[37] D. V. Matyushov and C. A. Angell, J. Chem. Phys. **126**, 094501 (2007).
[38] R. Tao and J. M. Sun, Phys. Rev. Lett. **67**, 398 (1991).
[39] J. M. Luttinger and L. Tisza, Phys. Rev. **70**, 954 (1946).
[40] M. S. S. Challa, D. P. Landau, and K. Binder, Phys. Rev. B **34**, 1841 (1986).
[41] A.-P. Hynninen and M. Dijkstra, Phys. Rev. Lett. **94**, 138303 (2005).
[42] D. Wei, Phys. Rev. E **49**, 2454 (1994).
[43] P. G. de Gennes and P. A. Pinkus, Phys. Kondens. Mater. **11**, 189 (1970).
[44] J. J. Weis, D. Levesque, and G. J. Zarragoicoechea, Phys. Rev. Lett. **69**, 913 (1992).
[45] E. LaNave, S. Mossa, and F. Sciortino, Phys. Rev. Lett. **88**, 225701 (2002).
[46] A. Heuer and S. Büchner, J. Phys.: Condens. Matter **12**, 6535 (2000).
[47] H. C. Andersen, D. Chandler, and J. D. Weeks, Adv. Chem. Phys. **34**, 105 (1976).
[48] M. S. Shell and P. G. Debenedetti, Phys. Rev. E **69**, 051102 (2004).
[49] H. Tanaka, Phys. Rev. E **62**, 6968 (2000).
[50] I. Saika-Voivod, P. H. Poole, and F. Sciortino, Nature (London) **412**, 514 (2001).
[51] S. Sastry and C. A. Angell, Nat. Mater. **2**, 739 (2003).
[52] L. Xu, P. Kumar, S. V. Buldyrev, S.-H. Chen, P. H. Poole, F. Sciortino, and H. E. Stanley, Proc. Natl. Acad. Sci. U.S.A. **102**, 16558 (2005).
[53] V. Molinero, S. Sastry, and C. A. Angell, Phys. Rev. Lett. **97**, 075701 (2006).
[54] A. V. Granato, J. Non-Cryst. Solids **307-310**, 376 (2002).
[55] J. P. Garrahan and D. Chandler, Proc. Natl. Acad. Sci. U.S.A. **100**, 9710 (2003).
[56] J. S. Langer, Phys. Rev. Lett. **97**, 115704 (2006).
[57] J. F. Douglas, J. Dudowicz, and K. F. Freed, J. Chem. Phys. **125**, 144907 (2006).
[58] T. B. Schroder, S. Sastry, J. C. Dyre, and S. C. Glotzer, J. Chem. Phys. **112**, 9834 (2000).
[59] L. E. Silbert, A. J. Liu, and S. R. Nagel, Phys. Rev. Lett. **95**, 098301 (2005).